

# Design of Self-supporting Surfaces

## Abstract

Self-supporting masonry is one of the most ancient and at the same time most elegant ways of building curved shapes. Their analysis and modeling is a topic of geometry processing rather than classical continuum mechanics, because of the very geometric nature of failure of such structures. In this paper we use the thrust network method of analysis and present an iterative nonlinear optimization algorithm for efficiently approximating freeform shapes by self-supporting ones. This provides an interactive modeling tool for such shapes. The rich geometry of thrust networks which was first studied by Maxwell in the 1860s leads us to new viewpoints of discrete differential geometry: We find close connections between different objects such as a finite-element discretization of the Airy stress potential, perfect graph Laplacians, and computing admissible loads via curvatures of polyhedral surfaces. This geometric viewpoint in particular shows us how to perform remeshing of a self-supporting shape by a self-supporting quad mesh with planar faces.

**CR Categories:** I.3.5 [Computer Graphics]: Computational Geometry and Object Modeling—Curve, surface, solid, and object representations;

**Keywords:** Discrete differential geometry, architectural geometry, self-supporting masonry, thrust networks, reciprocal force diagrams, discrete Laplace operators, isotropic geometry, mean curvature

## 1 Introduction

Vaulted masonry structures are among the simplest and at the same time most elegant solutions for creating curved shapes in building construction. This is the reason why they have been an object of interest since antiquity, large non-convex examples being provided by gothic cathedrals. They continue to be an active topic of research in today's engineering community.

Our paper is concerned with a combined geometry+statics analysis of *self-supporting* masonry and with tools for the interactive modeling of freeform self-supporting structures. Here “self-supporting” means that the structure, considered as an arrangement of blocks (bricks, stones), holds together by itself, and additional support, additional chains and similar are present only during construction. Our analysis is based on the following assumptions, which follow the classic [Heyman 1966]:

*Assumption 1:* Masonry has no tensile strength, but the individual building blocks do not slip against each other (because of friction or mortar). On the other hand, their compressive strength is sufficiently high so that failure of the structure is by a sudden change in geometry, such as shown by Figure 2, and not by material failure.

*Assumption 2 (The Safe Theorem):* If a system of forces can be found which is in equilibrium with the load on the structure and which is contained within the masonry envelope then the structure will carry the loads, although the actually occurring forces may not be those postulated.

Our approach is twofold: We first give an overview of the continuous case of a smooth surface under stress which turns out to be

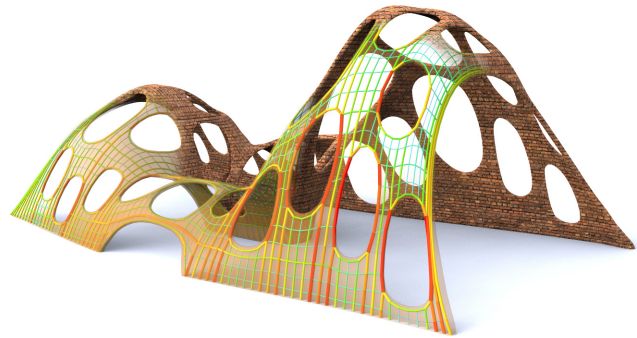


**Figure 1:** A surface with irregularly placed holes almost never stands by itself when built from bricks; for those that do, stability is not obvious by inspection. The surface shown is produced by finding the nearest self-supporting shape from a given freeform geometry. The image also illustrates the fictitious thrust network used in our algorithm, with edges' cross-section and coloring visualizing the magnitude of forces.

governed by the so-called Airy stress function, at least locally. This mathematical model is called a membrane in the engineering literature and has been applied to the analysis of masonry before. The surface is self-supporting if and only if stresses are entirely compressive (i.e., the Airy function is convex). For computational purposes, stresses are discretized as a fictitious *thrust network* [Block and Ochsendorf 2007] contained in the masonry structure. This is a system of forces which together with the structure's deadload is in equilibrium. It can be interpreted as a finite element discretization of the continuous case, and it turns out to have very interesting geometry dating back to the work of J. C. Maxwell [1864], with the Airy stress function becoming a polyhedral surface directly related to a reciprocal force diagram.

While previous work in architectural geometry was mostly concerned with aspects of rationalization and purely geometric side-conditions which occur in freeform architecture, the focus of this paper is design with *statics* constraints. In particular, our contributions are the following:

### Contributions.

- We connect the physics of self-supporting surfaces with vertical loads to the geometry of isotropic 3-space, with the direction of gravity as the distinguished direction (§2.3). Taking the convex Airy potential as unit sphere, one can express the equations governing self-supporting surfaces in terms of curvatures.
- We employ Maxwell's construction of polyhedral thrust networks and their reciprocal diagrams (§2.4), and give an interpretation of the equilibrium conditions in terms of discrete curvatures.
- The graph Laplacian derived from a thrust network with compressive forces is a “perfect” one (§2.2). We show how it appears in the analysis and establish a connection with mean curvatures which are otherwise defined for polyhedral surfaces.
- We present an optimization algorithm for efficiently finding a thrust network near a given arbitrary reference surface (§3), and build a tool for interactive design of self-supporting surfaces based on this algorithm (§4).

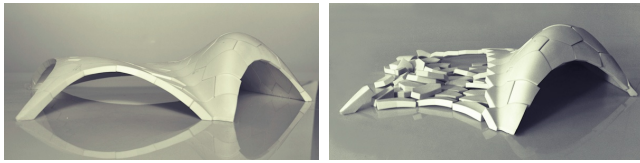


**Figure 2:** Masonry fails via geometric catastrophe rather than material failure (models by Block Research Group, ETH Zürich).

- We exploit the geometric relationships between a self-supporting surface and its stress potential in order to find particularly nice families of self-supporting surfaces, especially planar quadrilateral representations of thrust networks (§5).
- We demonstrate the versatility and applicability of our approach to the design and analysis of large-scale masonry and steel-glass structures.

**Related Work.** Unsupported masonry has been an active topic of research in the engineering community. The foundations for the modern approach were laid by Jacques Heyman [1966] and are available as the textbook [Heyman 1995]. A unifying view on polyhedral surfaces, compressive forces and corresponding “convex” force diagrams is presented by [Ash et al. 1988]. F. Fraternali [2002], [2010] established a connection between the continuous theory of stresses in membranes and the discrete theory of forces in thrust networks, by interpreting the latter as a certain non-conforming finite element discretization of the former.

Several authors have studied the problem of finding discrete compressive force networks contained within the boundary of masonry structures; early work in this area includes [Schek 1974], [Livesley 1992], and [O’Dwyer 1998]. Fraternali [2010] proposed solving for the structure’s discrete stress surface, and examining its convex hull to study the structure’s stability and susceptibility to cracking. Philippe Block’s seminal thesis introduced the method of *Thrust Network Analysis*, which linearizes the form-finding problem by first seeking a reciprocal diagram of the top view, which guarantees equilibrium of horizontal forces, then solving for the heights that balance the vertical loads (see e.g. [Block and Ochsendorf 2007; Block 2009]). Recent work by Block and coauthors extends this method in the case where the reciprocal diagram is not unique; for different choices of reciprocal diagram, the optimal heights can be found using the method of least squares [Van Mele and Block 2011], and the search for the best such reciprocal diagram can be automated using a genetic algorithm [Block and Lachauer 2011].

Other approaches to the interactive design of self-supporting structures include modeling these structures as damped particle-spring systems [Kilian and Ochsendorf 2005; Barnes 2009], and mirroring the rich tradition in architecture of designing self-supporting surfaces using hanging chain models [Heyman 1998]. Alternatively, masonry structures can be represented by networks of rigid blocks [Whiting et al. 2009], whose conditions on the structural feasibility were incorporated into procedural modeling of buildings.

Algorithmic and mathematical methods relevant to this paper are work on the geometry of quad meshes with planar faces [Glymph et al. 2004; Liu et al. 2006], discrete curvatures for such meshes [Pottmann et al. 2007; Bobenko et al. 2010], in particular curvatures in isotropic geometry [Pottmann and Liu 2007]. Schiftner and Balzer [2010] discuss approximating a reference surface by a quad mesh with planar faces, whose layout is guided by statics properties of that surface.

## 2 Self-supporting Surfaces

### 2.1 The Continuous Theory

We are here modeling masonry as a surface given by a height field  $s(x, y)$  defined in some planar domain  $\Omega$ . We assume that there are vertical loads  $F(x, y)$  — usually  $F$  represents the structure’s own weight. By definition this surface is self-supporting, if and only if there exists a field of compressive stresses which are in equilibrium with the acting forces. This is equivalent to existence of a field  $M(x, y)$  of  $2 \times 2$  symmetric positive semidefinite matrices satisfying

$$\operatorname{div}(M \nabla s) = F, \quad \operatorname{div} M = 0, \quad (1)$$

where the divergence operator  $\operatorname{div} \begin{pmatrix} u(x, y) \\ v(x, y) \end{pmatrix} = u_x + v_y$  is understood to act on the columns of a matrix (see e.g. [Fraternali 2010], [Giaquinta and Giusti 1985]).

The condition  $\operatorname{div} M = 0$  says that  $M$  is essentially the Hessian of a real-valued function  $\phi$  (the *Airy stress potential*): With the notation

$$M = \begin{pmatrix} m_{11} & m_{12} \\ m_{12} & m_{22} \end{pmatrix} \iff \widehat{M} = \begin{pmatrix} m_{22} & -m_{12} \\ -m_{12} & m_{11} \end{pmatrix}$$

it is clear that  $\operatorname{div} M = 0$  is an integrability condition for  $\widehat{M}$ , so locally there is a potential  $\phi$  with

$$\widehat{M} = \nabla^2 \phi, \quad \text{i.e.,} \quad M = \widehat{\nabla^2 \phi}.$$

If the domain  $\Omega$  is simply connected, this relation holds globally. Positive semidefiniteness of  $M$  (or equivalently of  $\widehat{M}$ ) characterizes *convexity* of the Airy potential  $\phi$ . The Airy function enters computations only by way of its derivatives, so global existence is not an issue.

*Remark:* Stresses at boundary points depend on the way the surface is anchored: A fixed anchor means no condition, but a free boundary with outer normal vector  $\mathbf{n}$  means  $\langle M \nabla s, \mathbf{n} \rangle = 0$ .

**Stress Laplacian.** Note that  $\operatorname{div} M = 0$  yields  $\operatorname{div}(M \nabla s) = \operatorname{tr}(M \nabla^2 s)$ , which we like to call  $\Delta_\phi s$ . The operator  $\Delta_\phi$  is symmetric. It is elliptic (as a Laplace operator should be) if and only if  $M$  is positive definite, i.e.,  $\phi$  is strictly convex. The balance condition (1) may be written as  $\Delta_\phi s = F$ .

### 2.2 Discrete Theory: Thrust Networks

We are discretizing a self-supporting surface by a mesh  $\mathcal{S} = (V, E, F)$  (see Figure 3). Loads are again vertical, and we discretize them as force densities  $F_i$  associated with vertices  $\mathbf{v}_i$ . The load acting on this vertex is then given by  $F_i A_i$ , where  $A_i$  is an area of influence (using a prime to indicate projection onto the  $xy$  plane,  $A_i$  is the area of the Voronoi cell of  $\mathbf{v}'_i$  w.r.t.  $V'$ ). We assume that stresses are carried by the edges of the mesh: the force exerted on the vertex  $\mathbf{v}_i$  by the edge connecting  $\mathbf{v}_i, \mathbf{v}_j$  is given by

$$w_{ij}(\mathbf{v}_j - \mathbf{v}_i), \quad \text{where} \quad w_{ij} = w_{ji} \geq 0.$$

The nonnegativity of the individual weights  $w_{ij}$  expresses the compressive nature of forces. The balance conditions at vertices then read as follows: With  $\mathbf{v}_i = (x_i, y_i, s_i)$  we have

$$\sum_{j \sim i} w_{ij} (x_j - x_i) = \sum_{j \sim i} w_{ij} (y_j - y_i) = 0, \quad (2)$$

$$\sum_{j \sim i} w_{ij} (s_j - s_i) = A_i F_i. \quad (3)$$

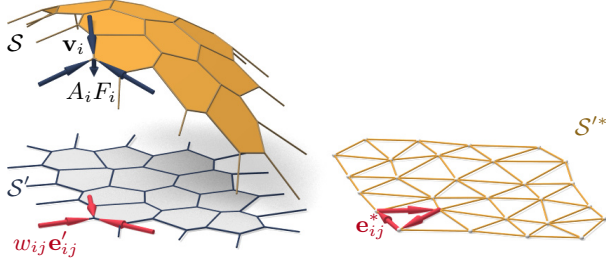


**Figure 3:** A thrust network  $\mathcal{S}$ , with dangling edges indicating external forces (left). This network together with compressive forces which balance vertical loads  $A_i F_i$  projects onto a planar mesh  $\mathcal{S}'$  with equilibrium compressive forces  $w_{ij} e'_{ij}$  in its edges. Rotating forces by  $90^\circ$  leads to the reciprocal force diagram  $\mathcal{S}'^*$  (right).

181 A mesh equipped with edge weights in this way is a discrete *thrust* 218 network. Invoking the safe theorem, we can state that a masonry 219 structure is self-supporting, if we can find a thrust network with 220 compressive forces which is entirely contained within the structure.

185 **Reciprocal Diagram.** Equations (2) have a geometric interpretation: With edge vectors 186

$$\mathbf{e}'_{ij} = \mathbf{v}'_j - \mathbf{v}'_i = (x_j, y_j) - (x_i, y_i),$$

187 Equation (2) asserts that vectors  $w_{ij} \mathbf{e}'_{ij}$  form a closed cycle. Rotating 188 them by 90 degrees, we see that likewise

$$\mathbf{e}''_{ij} = w_{ij} J \mathbf{e}'_{ij}, \quad \text{with } J = \begin{pmatrix} 0 & -1 \\ 1 & 0 \end{pmatrix},$$

189 form a closed cycle (see Figure 3). If the mesh  $\mathcal{S}$  is simply connected, 190 there exists an entire *reciprocal diagram*  $\mathcal{S}'^*$  which is a 191 combinatorial dual of  $\mathcal{S}$ , and which has edge vectors  $\mathbf{e}''_{ij}$ . Its 192 vertices are denoted by  $\mathbf{v}'^*$ .

193 *Remark:* If  $\mathcal{S}'$  is a Delaunay triangulation, then the corresponding 194 Voronoi diagram is an example of a reciprocal diagram.

195 **Polyhedral Stress Potential.** We can go further and construct a 196 convex polyhedral “Airy stress potential” surface  $\Phi$  with vertices 197  $\mathbf{w}_i = (x_i, y_i, \phi_i)$  combinatorially equivalent to  $\mathcal{S}$  by requiring that 198 a primal face of  $\Phi$  lies in the plane  $z = \alpha x + \beta y + \gamma$  if and only if 199  $(\alpha, \beta)$  is the corresponding dual vertex of  $\mathcal{S}'^*$  (see Figure 4). Ob- 200 viously this condition determines  $\Phi$  up to vertical translation. For 201 existence see [Ash et al. 1988]. The inverse procedure constructs 202 a reciprocal diagram from  $\Phi$ . This procedure works also if forces 203 are not compressive: we can construct an Airy mesh  $\Phi$  which has 204 planar faces, but it will no longer be a convex polyhedron.

205 The vertices of  $\Phi$  can be interpolated by a piecewise-linear function 206  $\phi(x, y)$ . It is easy to see that the derivative of  $\phi(x, y)$  jumps by the 207 amount  $\|\mathbf{e}''_{ij}\| = w_{ij} \|\mathbf{e}'_{ij}\|$ , when crossing over the edge  $\mathbf{e}'_{ij}$  at right 208 angle, with unit speed. This identifies  $\Phi$  as the Airy polyhedron in- 209 troduced by [Fraternali et al. 2002] as a finite element discretization 210 of the continuous Airy function (see also [Fraternali 2010]).

211 If the mesh is not simply connected, the reciprocal diagram and the 212 Airy polyhedron exist only locally. Global existence is not an issue 213 for our computations.

214 **Polarity.** Polarity with respect to the *Maxwell paraboloid*  $z =$  215  $\frac{1}{2}(x^2 + y^2)$  maps the plane  $z = \alpha x + \beta y + \gamma$  to the point  $(\alpha, \beta, -\gamma)$ . 216 Thus, applying polarity to  $\Phi$  and projecting the result  $\Phi^*$  into the  $xy$  217 plane reconstructs the reciprocal diagram  $\Phi'^* = \mathcal{S}'^*$  (see Fig. 4).

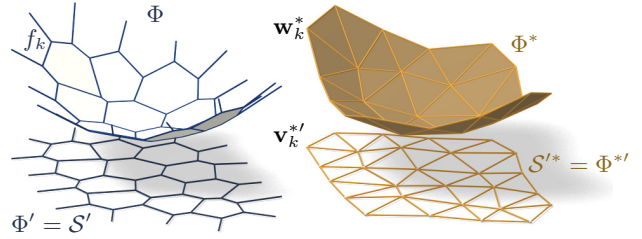


**Figure 4:** Airy stress potential  $\Phi$  and its polar dual  $\Phi^*$ .  $\Phi$  projects onto the same planar mesh as  $\mathcal{S}$  does, while  $\Phi^*$  projects onto the reciprocal force diagram. A primal face  $f_k$  lies in the plane  $z = \alpha x + \beta y + \gamma \iff$  the corresponding dual vertex is  $\mathbf{w}_k^* = (\alpha, \beta, -\gamma)$ .

218 **Discrete Stress Laplacian.** The weights  $w_{ij}$  may be used to define 219 a graph Laplacian  $\Delta_\phi$  which on vertex-based functions acts as

$$\Delta_\phi s(\mathbf{v}_i) = \sum_{j \sim i} w_{ij} (s_j - s_i).$$

220 This operator is a perfect discrete Laplacian in the sense of [War- 221 detzky et al. 2007], since it is symmetric by construction, Equa- 222 tion (2) implies linear precision for the planar “top view mesh”  $\mathcal{S}'$  223 (i.e.,  $\Delta_\phi f = 0$  if  $f$  is a linear function), and  $w_{ij} \geq 0$  ensures 224 semidefiniteness and a maximum principle for  $\Delta_\phi$ -harmonic func- 225 tions. Equation (3) can be written as  $\Delta_\phi s = AF$ .

226 Note that  $\Delta_\phi$  is well defined also in case the underlying meshes are 227 not simply connected.

### 228 2.3 Surfaces in Isotropic Geometry

229 It is worth while to reconsider the basics of self-supporting surfaces 230 in the language of dual-isotropic geometry, which takes place in  $\mathbb{R}^3$  231 with the  $z$  axis as a distinguished vertical direction. The basic ele- 232 ments of this geometry are planes, having equation  $z = f(x, y) =$  233  $\alpha x + \beta y + \gamma$ . The gradient vector  $\nabla f = (\alpha, \beta)$  determines the 234 plane up to translation. A plane tangent to the graph of the function 235  $s(x, y)$  has gradient vector  $\nabla s$ .

236 There is the notion of *parallel points*:  $(x, y, z) \parallel (x', y', z') \iff$  237  $x = x', y = y'$ .

238 *Remark:* The Maxwell paraboloid is considered the unit sphere of 239 isotropic geometry, and the geometric quantities considered above 240 are assigned specific meanings: The forces  $\|\mathbf{e}'_{ij}\| = w_{ij} \|\mathbf{e}_{ij}\|$  are 241 dihedral angles of the Airy polyhedron  $\Phi$ , and also “lengths” of 242 edges of  $\Phi^*$ . We do not use this terminology in the sequel.

243 **Curvatures.** Generally speaking, in the differential geometry of 244 surfaces one considers the *Gauss map*  $\sigma$  from a surface  $S$  to a con- 245 vex unit sphere  $\Phi$  by requiring that corresponding points have par- 246 allel tangent planes. Subsequently mean curvature  $H^{\text{rel}}$  and Gaus- 247 sian curvature  $K^{\text{rel}}$  relative to  $\Phi$  are computed from the derivative 248  $d\sigma$ . Classically  $\Phi$  is the ordinary unit sphere  $x^2 + y^2 + z^2 = 1$ , so 249 that  $\sigma$  maps each point its unit normal vector.

250 In our setting, parallelity is a property of *points* rather than planes, 251 and the Gauss map  $\sigma$  goes the other way, mapping the tangent 252 planes of the unit sphere  $z = \phi(x, y)$  to the corresponding tan- 253 gent plane of the surface  $z = s(x, y)$ . If we know which point a 254 plane is attached to, then it is determined by its gradient. So we 255 simply write

$$\nabla \phi \xrightarrow{\sigma} \nabla s.$$

By moving along a curve  $\mathbf{u}(t) = (x(t), y(t))$  in the parameter domain we get the first variation of tangent planes:  $\frac{d}{dt} \nabla \phi|_{\mathbf{u}(t)} = (\nabla^2 \phi)\dot{\mathbf{u}}$ . This yields the derivative  $(\nabla^2 \phi)\dot{\mathbf{u}} \stackrel{d\sigma}{\mapsto} (\nabla^2 s)\dot{\mathbf{u}}$ , for all  $\dot{\mathbf{u}}$ , and the matrix of  $d\sigma$  is found as  $(\nabla^2 \phi)^{-1}(\nabla^2 s)$ . By definition, curvatures of the surface  $s$  relative to  $\phi$  are found as

$$K_s^{\text{rel}} = \det(d\sigma) = \frac{\det \nabla^2 s}{\det \nabla^2 \phi},$$

$$H_s^{\text{rel}} = \frac{1}{2} \text{tr}(d\sigma) = \frac{1}{2} \text{tr} \left( \frac{\det \nabla^2 s}{\det \nabla^2 \phi} \nabla^2 \phi \right) = \frac{\Delta_\phi s}{2 \det \nabla^2 \phi}.$$

The Maxwell paraboloid  $\phi_0(x, y) = \frac{1}{2}(x^2 + y^2)$  is the canonical unit sphere of isotropic geometry, its Hessian equals  $E_2$ . Curvatures relative to  $\phi_0$  are not called “relative” and are denoted by the symbols  $H, K$  instead of  $H^{\text{rel}}, K^{\text{rel}}$ . The observation

$$\Delta_\phi \phi = \text{tr}(M \nabla^2 \phi) = \text{tr}(\widehat{\nabla^2 \phi} \nabla^2 \phi) = 2 \det \nabla^2 \phi$$

together with the formulas above implies

$$K_s = \det \nabla^2 s, \quad K_\phi = \det \nabla^2 \phi \implies H_s^{\text{rel}} = \frac{\Delta_\phi s}{2K_\phi} = \frac{\Delta_\phi s}{\Delta_\phi \phi}.$$

**Relation to Self-supporting Surfaces.** Summarizing the formulas above, we rewrite the balance condition (1) as

$$2K_\phi H_s^{\text{rel}} = \Delta_\phi s = F. \quad (4)$$

Let us draw some conclusions:

- Since  $H_\phi^{\text{rel}} = 1$  we see that the load  $F_\phi = 2K_\phi$  is admissible for the stress surface  $\phi(x, y)$ , which is hereby shown as self-supporting. The quotient of loads yields  $H_s^{\text{rel}} = F/F_\phi$ .
- If the stress surface coincides with the Maxwell paraboloid, then *constant loads characterize constant mean curvature surfaces*, because we get  $K_\phi = 1$  and  $H_s = F/2$ .
- If  $s_1, s_2$  have the same stress potential  $\phi$ , then  $H_{s_1-s_2}^{\text{rel}} = H_{s_1}^{\text{rel}} - H_{s_2}^{\text{rel}} = 0$ , so  $s_1 - s_2$  is a (relative) minimal surface.

## 2.4 Meshes in Isotropic Geometry

A general theory of curvatures of polyhedral surfaces with respect to a polyhedral unit sphere was proposed by [Pottmann et al. 2007; Bobenko et al. 2010], and its dual complement in isotropic geometry was elaborated by [Pottmann and Liu 2007]. As illustrated by Figure 5, the mean curvature of a self-supporting surface  $\mathcal{S}$  relative to its discrete Airy stress potential is associated with the vertices of  $\mathcal{S}$ . It is computed from areas and mixed areas of faces in the polar polyhedra  $\mathcal{S}^*$  and  $\Phi^*$ :

$$H^{\text{rel}}(\mathbf{v}_i) = \frac{A_i(\mathcal{S}, \Phi)}{A_i(\Phi, \Phi)}, \quad \text{where}$$

$$A_i(\mathcal{S}, \Phi) = \frac{1}{4} \sum_{k: f_k \in 1\text{-ring}(\mathbf{v}_i)} \det(\mathbf{v}'_k, \mathbf{w}'_{k+1}) + \det(\mathbf{w}'_k, \mathbf{v}'_{k+1}).$$

The prime denotes the projection into the  $xy$  plane, and summation is over those dual vertices which are adjacent to  $\mathbf{v}_i$ . Replacing  $\mathbf{v}'_k$  by  $\mathbf{w}'_k$  yields  $A_i(\Phi, \Phi) = \frac{1}{2} \sum \det(\mathbf{w}'_k, \mathbf{w}'_{k+1})$ .

**Proposition.** If  $\Phi$  is the Airy surface of a thrust network  $\mathcal{S}$ , then the mean curvature of  $\mathcal{S}$  relative to  $\Phi$  is computable as

$$H^{\text{rel}}(\mathbf{v}_i) = \frac{\sum_{j \sim i} w_{ij}(s_j - s_i)}{\sum_{j \sim i} w_{ij}(\phi_j - \phi_i)} = \frac{\Delta_\phi s}{\Delta_\phi \phi} \Big|_{\mathbf{v}_i}. \quad (5)$$

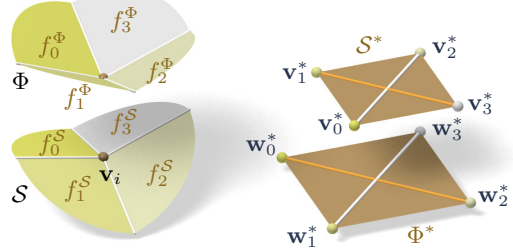


**Figure 5:** Mean curvature of a vertex  $\mathbf{v}_i$  of  $\mathcal{S}$ : Corresponding edges of the polar duals  $\mathcal{S}^*$ ,  $\Phi^*$  are parallel, and mean curvature according to [Pottmann et al. 2007] is computed from the vertices polar to faces adjacent to  $\mathbf{v}_i$ . For valence 4 vertices the case of zero mean curvature shown here is characterized by parallelity of non-corresponding diagonals of corresponding quads in  $\mathcal{S}^*$ ,  $\Phi^*$ .

**Proof.** It is sufficient to show  $2A_i(\mathcal{S}, \Phi) = \sum_{j \sim i} w_{ij}(s_j - s_i)$ .

For that, consider edges  $\mathbf{e}'_1, \dots, \mathbf{e}'_n$  emanating from  $\mathbf{v}'_i$ . The dual cycles in  $\Phi^{**}$  and  $\mathcal{S}^{**}$  without loss of generality are given by vertices  $(\mathbf{v}'_1^*, \dots, \mathbf{v}'_n^*)$  and  $(\mathbf{w}'_1^*, \dots, \mathbf{w}'_n^*)$ , respectively. The latter has edges  $\mathbf{w}'_{j+1} - \mathbf{w}'_j = w_{ij} J \mathbf{e}'_j$  (indices modulo  $n$ ).

Without loss of generality  $\mathbf{v}_i = 0$ , so the vertex  $\mathbf{v}'_j^*$  by construction equals the gradient of the linear function  $\mathbf{x} \mapsto \langle \mathbf{v}'_j^*, \mathbf{x} \rangle$  defined by the properties  $\mathbf{e}'_{j-1} \mapsto s_{j-1} - s_i$ ,  $\mathbf{e}'_j \mapsto s_j - s_i$ . Corresponding edge vectors  $\mathbf{v}'_{j+1} - \mathbf{v}'_j^*$  and  $\mathbf{w}'_{j+1} - \mathbf{w}'_j^*$  are parallel, because  $\langle \mathbf{v}'_{j+1} - \mathbf{v}'_j, \mathbf{e}'_j \rangle = (s_j - s_i) - (s_j - s_i) = 0$ . Expand  $2A_i(\mathcal{S}, \Phi)$ :

$$\begin{aligned} & \frac{1}{2} \sum \det(\mathbf{w}'_j, \mathbf{v}'_{j+1}) + \det(\mathbf{v}'_j, \mathbf{w}'_{j+1}) \\ &= \frac{1}{2} \sum \det(\mathbf{w}'_j - \mathbf{w}'_{j+1}, \mathbf{v}'_{j+1}) + \det(\mathbf{v}'_j, \mathbf{w}'_{j+1} - \mathbf{w}'_j) \\ &= \frac{1}{2} \sum \det(-w_{ij} J \mathbf{e}'_j, \mathbf{v}'_{j+1}) + \det(\mathbf{v}'_j, w_{ij} J \mathbf{e}'_j) \\ &= \sum \det(\mathbf{v}'_j, w_{ij} J \mathbf{e}'_j) = \sum w_{ij} \langle \mathbf{v}'_j, \mathbf{e}'_j \rangle = \sum w_{ij} (s_j - s_i). \end{aligned}$$

Here we have used  $\det(\mathbf{a}, J\mathbf{b}) = \langle \mathbf{a}, \mathbf{b} \rangle$ .  $\square$

In order to discretize (4), we also need a discrete Gaussian curvature, which is usually defined as a quotient of areas which correspond under the Gauss mapping. We define

$$K_\Phi(\mathbf{v}_i) = \frac{A_i(\Phi, \Phi)}{A_i},$$

where  $A_i$  is the Voronoi area of vertex  $\mathbf{v}'_i$  in the projected mesh  $\mathcal{S}'$  used in (3).

*Remark:* If the faces of the thrust network  $\mathcal{S}$  are not planar, the simple trick of introducing additional edges with zero forces in them makes them planar, and the theory is applicable. We refrain from elaborating this further.

**Discrete Balance Equation.** The discrete version of the balance equation (4) reads as follows:

**Theorem.** A simply-connected mesh  $\mathcal{S}$  with vertices  $\mathbf{v}_i = (x_i, y_i, s_i)$  can be put into static equilibrium with vertical forces “ $A_i F_i$ ” if and only if there exists a combinatorially equivalent mesh  $\Phi$  with planar faces and vertices  $(x_i, y_i, \phi_i)$ , such that curvatures of  $\mathcal{S}$  relative to  $\Phi$  obey

$$2K_\Phi(\mathbf{v}_i) H^{\text{rel}}(\mathbf{v}_i) = F_i \quad (6)$$

at every interior vertex and every free boundary vertex  $\mathbf{v}_i$ .  $\mathcal{S}$  can be put into compressive static equilibrium if and only if there exists a convex such  $\Phi$ .

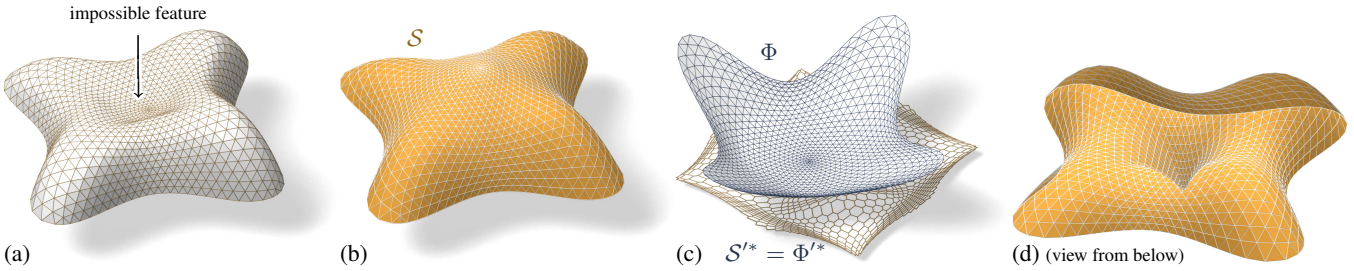


**Figure 6:** The top of the Lilium Tower (a) cannot stand as a masonry structure, because its central part is concave. Our algorithm finds a nearby self-supporting mesh (b) without this impossible feature. (c) shows the corresponding Airy mesh  $\Phi$  and reciprocal force diagram  $S'^*$ . (d) The user can edit the original surface, such as by specifying that the center of the surface is supported by a vertical pillar, and the self-supporting network adjusts accordingly.

Proof. The relation between equilibrium forces  $w_{ij}\mathbf{e}_{ij}$  in  $\mathcal{S}$  and the polyhedral stress potential  $\Phi$  has been discussed above, and so has the equivalence “ $w_{ij} \geq 0 \iff \Phi$  convex” (see e.g. [Ash et al. 1988] for a survey of this and related results). It remains to show that Equations (2) and (6) are equivalent. This is the case because the proposition above implies  $2K(\mathbf{v}_i)H^{\text{rel}}(\mathbf{v}_i) = 2\frac{A_i(\Phi, \Phi)}{A_i} \frac{A_i(\Phi, \mathcal{S})}{A_i(\Phi, \Phi)} = \frac{1}{A_i}(\sum_{j \sim i} w_{ij}(s_j - s_i)) = \frac{1}{A_i} A_i F_i$ .  $\square$

**Existence of Discretizations.** When considering discrete thrust networks as discretizations of continuous self-supporting surfaces, the following question is important: For a given smooth surface  $s(x, y)$  with Airy stress function  $\phi$ , does there exist a polyhedral surface  $\mathcal{S}$  in equilibrium approximating  $s(x, y)$ , whose top view is a given planar mesh  $\mathcal{S}'$ ? We restrict our attention to triangle meshes, where planarity of the faces of the discrete stress surface  $\Phi$  is not an issue. This question has several equivalent reformulations:

- Does  $\mathcal{S}'$  have a reciprocal diagram whose corresponding Airy polyhedron  $\Phi$  approximates the continuous Airy potential  $\phi$ ? (if the surfaces involved are not simply connected, these objects are defined locally).
- Does  $\mathcal{S}'$  possess a “perfect” discrete Laplace-Beltrami operator  $\Delta_\phi$  in the sense of Wardetzky et al. [2007] whose weights are the edge length scalars of such a reciprocal diagram?

From [Wardetzky et al. 2007] we know that perfect Laplacians exist only on regular triangulations which are projections of convex polyhedra. On the other hand, previous sections show how to appropriately re-triangulate: Let  $\Phi$  be a triangle mesh convex hull of the vertices  $(x_i, y_i, \phi(x_i, y_i))$ , where  $(x_i, y_i)$  are vertices of  $\mathcal{S}'$ . Then its polar dual  $\Phi^*$  projects onto a reciprocal diagram with positive edge weights, so  $\Delta_\phi$  has positive weights, and the vertices  $(x_i, y_i, s_i)$  of  $\mathcal{S}$  can be found by solving the discrete Poisson problem  $(\Delta_\phi s)_i = A_i F_i$ .

Assuming the discrete  $\Delta_\phi$  approximates its continuous counterpart, this yields a mesh approximating  $s(x, y)$ , and we conclude: A smooth self-supporting surface can be approximated by a discrete self-supporting triangular mesh for any sampling of the surface.

### 3 Thrust Networks from Reference Meshes

Consider now the problem of taking a given reference mesh, say  $\mathcal{R}$ , and finding a combinatorially equivalent mesh  $\mathcal{S}$  in static equilibrium approximating  $\mathcal{R}$ . The loads on  $\mathcal{S}$  include user-prescribed loads as well as the dead load caused by the mesh’s own weight. Conceptually, finding  $\mathcal{S}$  amounts to minimizing some formulation of distance between  $\mathcal{R}$  and  $\mathcal{S}$ , subject to constraints (2), (3), and  $w_{ij} \geq 0$ . For any choice of distance this minimization will be a nonlinear, non-convex, inequality-constrained variational problem

that cannot be efficiently solved in practice. Instead we propose a staggered optimization algorithm:

0. Start with an initial guess  $\mathcal{S} = \mathcal{R}$ .
1. Estimate the self-load on the vertices of  $\mathcal{S}$ , using their current positions.
2. Fixing  $\mathcal{S}$ , fit an associated stress surface  $\Phi$ .
3. Alter positions  $\mathbf{v}_i$  to improve the fit.
4. Repeat from Step 1 until convergence.

**Step 1: Estimating Self-Load.** The dead load due to the surface’s own weight depends not only on the top view of  $\mathcal{S}$ , but also on the surface area of its faces. To avoid adding nonlinearity to the algorithm, we estimate the load coefficients  $F_i$  at the beginning of each iteration, and assume they remain constant until the next iteration. We estimate the load “ $A_i F_i$ ” associated with each vertex by calculating its Voronoi area on each of its incident faces, and then multiplying by a user-specified surface density  $\rho$ .

**Step 2: Fit a Stress Surface.** In this step, we fix  $\mathcal{S}$  and try to fit a stress surface  $\Phi$  subordinate to the top view  $\mathcal{S}'$  of the primal mesh. We do so by searching for dihedral angles between the faces of  $\Phi$  which minimize, in the least-squares sense, the error in force equilibrium (6) and local integrability of  $\Phi$ . Doing so is equivalent to minimizing the squared residuals of Equations (3) and (2), respectively, with the positions held fixed. Defining the *equilibrium energy*

$$E = \sum_i \left\| \begin{pmatrix} 0 \\ 0 \\ A_i F_i \end{pmatrix} - \sum_{j \sim i} w_{ij} (\mathbf{v}_j - \mathbf{v}_i) \right\|^2, \quad (7)$$

where the outer sum is over the interior and free boundary vertices, we solve

$$\min_{w_{ij}} E, \quad \text{s.t. } 0 \leq w_{ij} \leq w_{\max}. \quad (8)$$

Here  $w_{\max}$  is an optional maximum weight we are willing to assign (to limit the amount of stress in the surface). This convex, sparse, box-constrained least-squares problem [Friedlander 2007] always has a solution. If the objective is 0 at this solution, the faces of  $\Phi$  locally integrate to a stress surface satisfying (6), and so  $\Phi$  certifies that  $\mathcal{S}$  is self-supporting – we are done. Otherwise,  $\mathcal{S}$  is not self-supporting and its vertices must be moved.

**Step 3: Alter Positions.** In the previous step we fit as best as possible a stress surface  $\Phi$  to  $\mathcal{S}$ . There are two possible kinds of error with this fit: the faces around a vertex (equivalently, the reciprocal diagram) might not close up; and the resulting stress forces might not be exactly in equilibrium with the loads. These errors

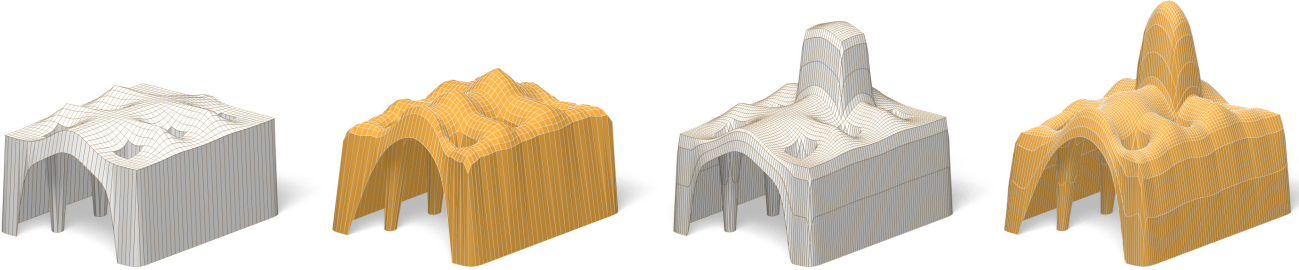


**Figure 7:** The user-designed reference mesh (left) is not self-supporting, but our algorithm finds a nearby perturbation of the reference surface (middle-left) that is in equilibrium. As the user makes edits to the reference surface (middle-right), the thrust network automatically adjusts (right).

403 can be decreased by modifying the top view and heights of  $\mathcal{S}$ , re-  
404 spectively. It is possible to simply solve for new vertex positions  
405 that put  $\mathcal{S}$  in static equilibrium, since Equations (2) and (3) with  
406  $w_{ij}$  fixed form a square linear system that is typically nonsingular.

407 While this approach would yield a self-supporting  $\mathcal{S}$ , this mesh is  
408 often far from the reference mesh  $\mathcal{R}$ , since any local errors in the  
409 stress surface from Step 2 amplify into global errors in  $\mathcal{S}$ . We pro-  
410 pose instead to look for new positions that decrease the imbalance  
411 in the stresses and loads, while also penalizing drift away from the  
412 reference mesh:

$$\min_{\mathbf{v}} E + \alpha \sum_i \langle \mathbf{n}_i, \mathbf{v}_i - \mathbf{v}_i^0 \rangle^2 + \beta \|\mathbf{v} - \mathbf{v}_P^0\|^2,$$

413 where  $\mathbf{v}_i^0$  is the position of the  $i$ -th vertex at the start of this step  
414 of the optimization,  $\mathbf{n}_i$  is the starting vertex normal (computed as  
415 the average of the incident face normals),  $\mathbf{v}_P^0$  is the projection of  $\mathbf{v}^0$   
416 onto the reference mesh, and  $\alpha > \beta$  are penalty coefficients that are  
417 decreased every iteration of Steps 1–3 of the algorithm. The second  
418 term allows  $\mathcal{S}$  to slide over itself (if doing so improves equilibrium)  
419 but penalizes drift in the normal direction. The third term, weaker  
420 than the second, regularizes the optimization by preventing large  
421 drift away from the reference surface or excessive tangential slid-  
422 ing.

423 **Implementation Details.** Solving the weighted least-squares  
424 problem of Step 3 amounts to solving a sparse, symmetric linear  
425 system. While the MINRES algorithm [Paige and Saunders 1975]  
426 is likely the most robust algorithm for solving this system, in prac-  
427 tice we have observed that the method of conjugate gradients works  
428 well despite the potential ill-conditioning of the objective matrix.

429 **Limitations.** This algorithm is not guaranteed to always con-  
430 verge; this fact is not surprising from the physics of the problem  
431 (if the boundary of the reference mesh encloses too large of a re-  
432 gion,  $w_{\max}$  is set too low, and the density of the surface too high,  
433 a thrust network in equilibrium simply does not exist – the vault is  
434 too ambitious and cannot be built to stand; pillars are needed.)

435 We can, however, make a few remarks. Step 2 always decreases the  
436 equilibrium energy  $E$  of Equation (7) and Step 3 does as well as  
437  $\beta \rightarrow 0$ . Moreover, as  $\alpha \rightarrow 0$  and  $\beta \rightarrow 0$ , Step 3 approaches a lin-  
438 ear system with as many equations as unknowns; if this system has  
439 full rank, its solution sets  $E = 0$ . These facts suggest that the algo-  
440 rithm should generally converge to a thrust network in equilibrium,  
441 provided that Step 1 does not increase the loads by too much at ev-  
442 ery iteration, and this is indeed what we observe in practice. One  
443 case where this assumption is guaranteed to hold is if the thickness  
444 of the surface is allowed to freely vary, so that it can be chosen so  
445 that the surface has uniform density over the top view.

446 If the linear system in Step 3 is singular and infeasible, the algo-  
447 rithm can stall at  $E > 0$ . This failure occurs, for instance, when  
448 an interior vertex has height  $z_i$  lower than all of its neighbors, and  
449 Step 2 assigns all incident edges to that vertex a weight of zero:  
450 clearly no amount of moving the vertex or its neighbors can bring  
451 the vertex into equilibrium. We avoid such degenerate configura-  
452 tions by bounding weights slightly away from zero in (8), trading  
453 increased robustness for slight smoothing of the resulting surface.

## 4 Results

455 **Interactive Design of Self-Supporting Surfaces.** The opti-  
456 mization algorithm described in the previous section forms the ba-  
457 sis of an interactive design tool for self-supporting surfaces. Users  
458 manipulate a mesh representing a reference surface, and the com-  
459 puter searches for a nearby thrust network in equilibrium (see e.g.  
460 Figure 7). Fitting this thrust network does not require that the user  
461 specify boundary tractions, and although the top view of the refer-  
462 ence mesh is used as an initial guess for the top view of the thrust  
463 network, the search is not restricted to this top view. The features  
464 of the design tool include:

- 465 • Handle-based 3D editing of the reference mesh using Lapla-  
466 cian coordinates [Lipman et al. 2004; Sorkine et al. 2003] to  
467 extrude vaults, insert pillars, and apply other deformations to  
468 the reference mesh. Handle-based adjustments of the heights,  
469 keeping the top view fixed, and deformation of the top view,  
470 keeping the heights fixed, are also supported. The thrust net-  
471 work adjusts interactively to fit the deformed positions, giving  
472 the usual visual feedback about the effects of edits on whether  
473 or not the surface can stand.
- 474 • Specification of boundary conditions. Points of contact be-  
475 tween the reference surface and the ground or environment  
476 are specified by “pinning” vertices of the surface, specifying  
477 that the thrust network must coincide with the reference mesh  
478 at this point, and relaxing the condition that forces must be in  
479 equilibrium there.
- 480 • Interactive adjustment of surface density  $\rho$ , external loads,  
481 and maximum permissible stress per edge  $w_{\max}$ , with visual  
482 feedback of how these parameters affect the fitted thrust net-  
483 work.
- 484 • Upsampling of the thrust network through Catmull-Clark sub-  
485 division and polishing of the resulting refined thrust network  
486 using optimization (§3).
- 487 • Visualization of the stress surface dual to the thrust network  
488 and corresponding reciprocal diagram.

489 **Example: Vault with Pillars.** As an example of the design and  
490 optimization workflow, consider a rectangular vault with six pillars,  
491 free boundary conditions along one edge, fixed boundary conditions

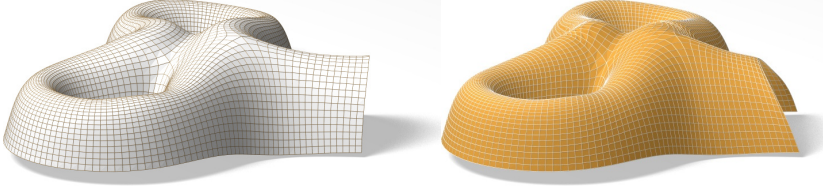


**Figure 8:** A freeform surface (left) needs adjustments around the entrance arch and between the two pillars in order to be self-supporting; our algorithm finds the nearby surface in equilibrium (right) that incorporates these changes.

Example	Figure	Vertices	Edges	Time (s)	Iterations	Max Rel Error
Top of Lilium Tower	Fig. 6b	1201	3504	21.6	9	$4.2 \times 10^{-5}$
Top of Lilium Tower (with pillar)	Fig. 6d	1200	3500	26.5	10	$8.5 \times 10^{-5}$
Freeform Structure with Two Pillars	Fig. 8	1535	2976	17.0	21	$2.7 \times 10^{-5}$
Swiss Cheese	Fig. 9	2358	4302	19.5	9	$3.0 \times 10^{-4}$
Brick Domes	Fig. 13	752	2165	8.0	9	$5.8 \times 10^{-5}$
Structural Glass	Fig. 16	527	998	5.7	25	$2.4 \times 10^{-5}$

**Table 1:** Numerical details about the examples throughout this paper. Time: The wall-clock time needed by an Intel Xeon 2.3GHz desktop PC with 4 GB of RAM to find a self-supporting thrust network and associated stress surface from the example’s reference mesh; we also give the number of outer iterations of the four steps in (§3). The maximum relative error is the dimensionless relative error in force equilibrium defined by  $\max_i \|A_i F_i - \sum_{j \sim i} w_{ij}(\mathbf{v}_j - \mathbf{v}_i)\| / \|A_i F_i\|$ , where the maximum is taken runs over interior vertices  $\mathbf{v}_i$ .

along the others, and a tower extruded from the top of the surface (see Figure 7). This surface is neither convex nor simply connected, and exhibits a mix of boundary conditions, none of which cause our algorithm any difficulty; it finds a self-supporting thrust network near the designed reference mesh. The user is now free to make edits to the reference mesh, and the thrust network adapts to these edits, providing the user feedback on whether these designs are physically realizable.

**Example: Top of the Lilium Tower.** Consider the top portion of the steel-glass exterior surface of the Lilium Tower, which is currently being built in Warszaw (see Figure 6). This surface contains a concave part with local minimum in its interior and so cannot possibly be self-supporting. Given this surface as a reference mesh, our algorithm constructs a nearby thrust network in equilibrium without the impossible feature. The user can then explore how editing the reference mesh – adding a pillar, for example – affects the thrust network and its deviation from the reference surface.

**Example: Freeform Structure with Two Pillars.** Suppose an architect’s experience and intuition has permitted the design of a freeform surface (see Figure 8) that is nearly self-supporting. Our algorithm reveals those edits needed to make the structure sound – principally around the entrance arch, and the area between the two pillars.

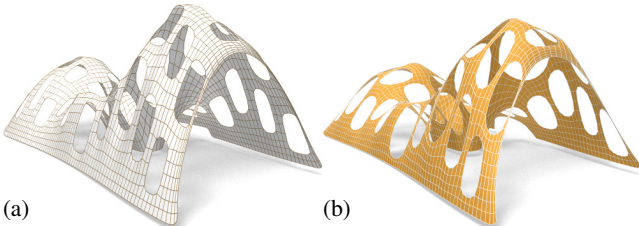


**Figure 9:** A mesh with holes (a) requires large deformations to both the top view and heights to render it self-supporting (b)

**Example: Swiss Cheese.** Cutting holes in a self-supporting surface interrupts force flow lines and causes dramatic global changes to the surface stresses, often to the point that the surface is no longer in equilibrium. Whether a given surface with many such holes can stand is far from obvious. Figure 9 shows such an implausible and unstable surface; our optimization finds a nearby, equally implausible but stable surface without difficulty (see Figures 1 and 9).

## 5 Special Self-Supporting Surfaces

**PQ Meshes.** Meshes with *planar* faces are of particular interest in architecture, so in this section we discuss how to remesh a given thrust network in equilibrium such that it becomes a quad mesh with planar faces (again in equilibrium). If this mesh is realized as a steel-glass construction, it is self-supporting in its beams alone, with no forces exerted on the glass (this is the usual manner of using glass). The beams constitute a self-supporting structure which is in perfect force equilibrium (without moments in the nodes) if only the deadload is applied.



**Figure 10:** Directly enforcing planarity of the faces of even a very simple self-supporting quad-mesh vault (a) results in a surface far removed from the original design (b). Starting instead from a remeshing of the surface with edges following relative principal curvature directions yields a self-supporting, PQ mesh far more faithful to the original (c).

Taking an arbitrary non-planar quad mesh and attempting naive, simultaneous enforcement of planarity and static equilibrium does not yield good results, as shown in Figure 10. To identify the necessary conditions, we first discuss a planar quad mesh  $\mathcal{S}$  with vertices  $\mathbf{v}_{ij} = (x_{ij}, y_{ij}, s_{ij})$  which approximates a given continuous surface  $s(x, y)$ . It is known that  $\mathcal{S}$  must approximately follow a network of conjugate curves in the surface (see e.g. [Liu et al. 2006]).

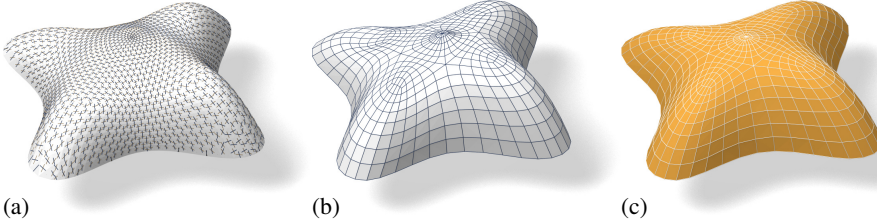


**Figure 11:** Planar quad remeshing of the “Lilium tower” surface of Figure 6. (a) Principal directions which are found as eigenvectors of  $(\nabla^2\phi)^{-1}\nabla^2s$ . (b) Quad mesh guided by principal directions is almost planar and almost self-supporting. (c) Small changes achieve both properties.

We can derive this condition in an elementary way as follows: Using a Taylor expansion, we compute the volume of the convex hull of the quadrilateral  $\mathbf{v}_{ij}, \mathbf{v}_{i+1,j}, \mathbf{v}_{i+1,j+1}, \mathbf{v}_{i,j+1}$ , assuming the vertices lie exactly on the surface  $s(x, y)$ . This results in

$$\text{vol} = \frac{1}{6} \det(\mathbf{a}_1, \mathbf{a}_2) \cdot ((\mathbf{a}_1)^T \nabla^2 s \mathbf{a}_2) + \dots,$$

where  $\mathbf{a}_1 = \begin{pmatrix} x_{i+1,j} - x_{ij} \\ y_{i+1,j} - y_{ij} \end{pmatrix}$ ,  $\mathbf{a}_2 = \begin{pmatrix} x_{i,j+1} - x_{ij} \\ y_{i,j+1} - y_{ij} \end{pmatrix}$ ,

and the dots indicate higher order terms. We see that planarity requires  $(\mathbf{a}_1)^T \nabla^2 s \mathbf{a}_2 = 0$ . In addition to the mesh  $\mathcal{S}$  approximating the surface  $s(x, y)$ , the corresponding polyhedral Airy surface  $\Phi$  must approximate  $\phi(x, y)$ ; thus we get the conditions

$$(\mathbf{a}_1)^T \nabla^2 s \mathbf{a}_2 = (\mathbf{a}_1)^T \nabla^2 \phi \mathbf{a}_2 = 0.$$

$\mathbf{a}_1, \mathbf{a}_2$  are therefore eigenvectors of  $(\nabla^2\phi)^{-1}\nabla^2s$ . In view of §2.3,  $\mathbf{a}_1, \mathbf{a}_2$  indicate the principal directions of the surface  $s(x, y)$  relative to  $\phi(x, y)$ .

In the discrete case, where  $s, \phi$  are not given as continuous surfaces, but are represented by a mesh in equilibrium and its Airy mesh, we use the techniques of Schiftner [2007] and Cohen-Steiner and Morvan [2003] to approximate the Hessians  $\nabla^2 s, \nabla^2 \phi$ , compute principal directions as eigenvectors of  $(\nabla^2\phi)^{-1}\nabla^2s$ , and subsequently find meshes  $\mathcal{S}, \Phi$  approximating  $s, \phi$  which follow those directions. Global optimization now makes  $\mathcal{S}, \Phi$  a valid thrust network with discrete stress potential. Convexity of  $\Phi$  ensures that  $\mathcal{S}$  is self-supporting.

Note that the relative principal curvature directions give the *unique* curve network along which a planar quad discretization of a self-supporting surface is possible. Other networks lead to results like the one shown by Figure 10. Figures 11 and 14 further illustrate the result of applying this procedure to self-supporting surfaces.

*Remark:* When remeshing a given shape by planar quad meshes, we know that the circular and conical properties require that the mesh follows the ordinary, Euclidean principal curvature directions [Liu et al. 2006]. It is remarkable that the self-supporting property in a similar manner requires us to follow certain *relative* principal directions. Practitioners’ observations regarding the beneficial statics properties of principal directions can be explained by this analogy, because the relative principal directions are close to the Euclidean ones, if the stress distribution is uniform and  $\|\nabla s\|$  is small.

**Koenigs Meshes.** Given a self-supporting thrust network  $\mathcal{S}$  with stress surface  $\Phi$ , we ask the question: Which vertical perturbation  $\mathcal{S} + \mathcal{R}$  is self-supporting, with the same loads as  $\mathcal{S}$ ? As to notation, all involved meshes  $\mathcal{S}, \mathcal{R}, \Phi$  have the same top view, and arithmetic operations refer to the respective  $z$  coordinates  $s_i, r_i, \phi_i$  of vertices.

The condition of equal loads then is expressed as  $\Delta_\phi(s + r) = \Delta_\phi s$  in terms of Laplacians or as  $H_S^{\text{rel}} = H_{S+\mathcal{R}}^{\text{rel}}$  in terms of mean curvature, and is equivalent to

$$\Delta_\phi r = 0, \quad \text{i.e.,} \quad H_{\mathcal{R}}^{\text{rel}} = 0.$$

So  $\mathcal{R}$  is a *minimal surface* relative to  $\Phi$ . While in the triangle mesh case there are enough degrees of freedom for nontrivial solutions, the case of planar quad meshes is more intricate: Polar polyhedra  $\mathcal{R}^*, \Phi^*$  have to be Christoffel duals of each other [Pottmann and Liu 2007], as illustrated by Figure 5. Unfortunately not all quad meshes have such a dual; the condition is that the mesh is *Koenigs*, i.e., the derived mesh formed by the intersection points of diagonals of faces again has planar faces [Bobenko and Suris 2008].



**Figure 12:** A “Koebe” mesh  $\Phi$  is self-supporting for unit dead load. An entire family of self-supporting meshes with the same top view is defined by  $\mathcal{S}_\alpha = \Phi + \alpha\mathcal{R}$ , where  $\mathcal{R}$  is chosen as  $\Phi$ ’s Christoffel-dual.

**Koebe meshes.** An interesting special case occurs if  $\Phi$  is a *Koebe* mesh of isotropic geometry, i.e., a PQ mesh whose edges touch the Maxwell paraboloid. Since  $\Phi$  approximates the Maxwell paraboloid, we get  $2K(\mathbf{v}_i)H^{\text{rel}}(\mathbf{v}_i) \approx 1$  and  $\Phi$  consequently is self-supporting for unit load. Applying the Christoffel dual construction described above yields a minimal mesh  $\mathcal{R}$  and a family of meshes  $\Phi + \alpha\mathcal{R}$  which are self-supporting for unit load (see Figure 12).

## 6 Conclusion and Future Work

**Conclusion.** This paper builds on relations between statics and geometry, some of which have been known for a long time, and connects them with newer methods of discrete differential geometry, such as discrete Laplace operators and curvatures of polyhedral surfaces. We were able to find efficient ways of modeling self-supporting freeform shapes, and provide architects and engineers with an interactive tool which gives quick information on the statics of freeform geometries. The self-supporting property of a shape is directly relevant for freeform masonry. The actual thrust networks we use for computation are relevant e.g. for steel constructions, where equilibrium of deadload forces implies absence of moments. This theory and accompanying algorithms thus constitute a new contribution to architectural geometry, connecting statics and geometric design.

**Future Work.** There are several directions of future research. One is to incorporate non-manifold meshes, which occur naturally when e.g. supporting walls are introduced. It is also obvious that non-vertical loads, e.g. wind load, play a role. There are also some directions to pursue in improving the algorithms, for instance adaptive remeshing in problem areas. Probably the interesting connections between statics properties and geometry are not yet exhausted, and

619 we would like to propose the *geometrization* of problems as a strat-  
620 egy for their solution.

671 LIPMAN, Y., SORKINE, O., COHEN-OR, D., LEVIN, D., ROSSI,  
672 C., AND SEIDEL, H. 2004. Differential coordinates for interac-  
673 tive mesh editing. In *Proc. SMI*. IEEE, 181–190.

## References

- 622 ASH, P., BOLKER, E., CRAPO, H., AND WHITELEY, W. 1988.  
623 Convex polyhedra, Dirichlet tessellations, and spider webs. In  
624 *Shaping space (Northampton 1984)*. Birkhäuser, 231–250.
- 625 BARNES, M. R. 2009. Form finding and analysis of tension struc-  
626 tures by dynamic relaxation. *Int. J. Space Structures* 14, 2, 89–  
627 104.
- 628 BLOCK, P., AND LACHAUER, L. 2011. Closest-fit, compression-  
629 only solutions for free form shells. In *IABSE—IASS 2011 Lon-  
630 don Symposium*, Int. Ass. Shell Spatial Structures. electronic.
- 631 BLOCK, P., AND OCHSENDORF, J. 2007. Thrust network analysis:  
632 A new methodology for three-dimensional equilibrium. *J. Int.  
633 Assoc. Shell and Spatial Structures* 48, 3, 167–173.
- 634 BLOCK, P. 2009. *Thrust Network Analysis: Exploring Three-  
635 dimensional Equilibrium*. PhD thesis, Massachusetts Institute  
636 of Technology.
- 637 BOBENKO, A., AND SURIS, YU. 2008. *Discrete differential geom-  
638 etry: Integrable Structure*. No. 98 in Graduate Studies in Math.  
639 American Math. Soc.
- 640 BOBENKO, A., POTTMANN, H., AND WALLNER, J. 2010. A  
641 curvature theory for discrete surfaces based on mesh parallelity.  
642 *Math. Annalen* 348, 1–24.
- 643 COHEN-STEINER, D., AND MORVAN, J.-M. 2003. Restricted  
644 Delaunay triangulations and normal cycle. In *Proc. 19th Symp.  
645 Computational geometry*, ACM, 312–321.
- 646 FRATERNALI, F., ANGELILLO, M., AND FORTUNATO, A. 2002.  
647 A lumped stress method for plane elastic problems and the  
648 discrete-continuum approximation. *Int. J. Solids Struct.* 39,  
649 6211–6240.
- 650 FRATERNALI, F. 2010. A thrust network approach to the equi-  
651 librium problem of unreinforced masonry vaults via polyhedral  
652 stress functions. *Mechanics Res. Comm.* 37, 2, 198 – 204.
- 653 FRIEDLANDER, M. P., 2007. BCLS: Bound constrained least  
654 squares. <http://www.cs.ubc.ca/~mpf/bcls>.
- 655 GIAQUINTA, M., AND GIUSTI, E. 1985. Researches on the equi-  
656 librium of masonry structures. *Archive for Rational Mechanics  
657 and Analysis* 88, 4, 359–392.
- 658 GLYMPH, J., SHELDEN, D., CECCATO, C., MUSSEL, J., AND  
659 SCHOBER, H. 2004. A parametric strategy for free-form glass  
660 structures using quadrilateral planar facets. *Automation in Con-  
661 struction* 13, 2, 187 – 202.
- 662 HEYMAN, J. 1966. The stone skeleton. *Int. J. Solids Structures* 2,  
663 249–279.
- 664 HEYMAN, J. 1995. *The Stone Skeleton: Structural Engineering of  
665 Masonry Architecture*. Cambridge University Press.
- 666 HEYMAN, J. 1998. *Structural Analysis: A Historical Approach*.  
667 Cambridge University Press.
- 668 KILIAN, A., AND OCHSENDORF, J. 2005. Particle-spring sys-  
669 tems for structural form finding. *J. Int. Assoc. Shell and Spatial  
670 Structures* 46, 77–84.
- 674 LIU, Y., POTTMANN, H., WALLNER, J., YANG, Y.-L., AND  
675 WANG, W. 2006. Geometric modeling with conical meshes  
676 and developable surfaces. *ACM Trans. Graph.* 25, 3, 681–689.
- 677 LIVESLEY, R. K. 1992. A computational model for the limit anal-  
678 ysis of three-dimensional masonry structures. *Meccanica* 27,  
679 161–172.
- 680 MAXWELL, J. 1864. On reciprocal diagrams and diagrams of  
681 forces. *Philosophical Magazine* 4, 27, 250–261.
- 682 O'Dwyer, D. 1998. Funicular analysis of masonry vaults. *Com-  
683 puters and Structures* 73, 187–197.
- 684 PAIGE, C. C., AND SAUNDERS, M. A. 1975. Solution of sparse  
685 indefinite systems of linear equations. *SIAM J. Num. Analysis*  
686 12, 617–629.
- 687 POTTMANN, H., AND LIU, Y. 2007. Discrete surfaces in isotropic  
688 geometry. In *Mathematics of Surfaces XII*, M. Sabin and J. Win-  
689 kler, Eds., vol. 4647 of *LNCS*. Springer-Verlag, 341–363.
- 690 POTTMANN, H., LIU, Y., WALLNER, J., BOBENKO, A., AND  
691 WANG, W. 2007. Geometry of multi-layer freeform structures  
692 for architecture. *ACM Trans. Graphics* 26, 3, #65,1–11.
- 693 SCHEK, H.-J. 1974. The force density method for form finding and  
694 computation of general networks. *Computer Methods in Applied  
695 Mathematics and Engineering* 3, 115–134.
- 696 SCHIFTNER, A., AND BALZER, J. 2010. Statics-sensitive layout  
697 of planar quadrilateral meshes. In *Advances in Architectural Ge-  
698 ometry 2010*, C. Ceccato et al., Eds. Springer, Vienna, 221–236.
- 699 SCHIFTNER, A. 2007. *Planar quad meshes from relative principal  
700 curvature lines*. Master's thesis, TU Wien.
- 701 SORKINE, O., COHEN-OR, D., AND TOLEDO, S. 2003. High-  
702 pass quantization for mesh encoding. In *Symposium Geometry  
703 processing*. Eurographics Assoc., 42–51.
- 704 VAN MELE, T., AND BLOCK, P. 2011. A novel form finding  
705 method for fabric formwork for concrete shells. *J. Int. Assoc.  
706 Shell and Spatial Structures* 52, 217–224.
- 707 WARDETZKY, M., MATHUR, S., KÄLBERER, F., AND GRIN-  
708 SPUN, E. 2007. Discrete Laplace operators: No free lunch.  
709 In *Symposium on Geometry Processing*, 33–37.
- 710 WHITING, E., OCHSENDORF, J., AND DURAND, F. 2009. Proce-  
711 dural modeling of structurally-sound masonry buildings. *ACM  
712 Trans. Graph.* 28, 5, #112,1–9.

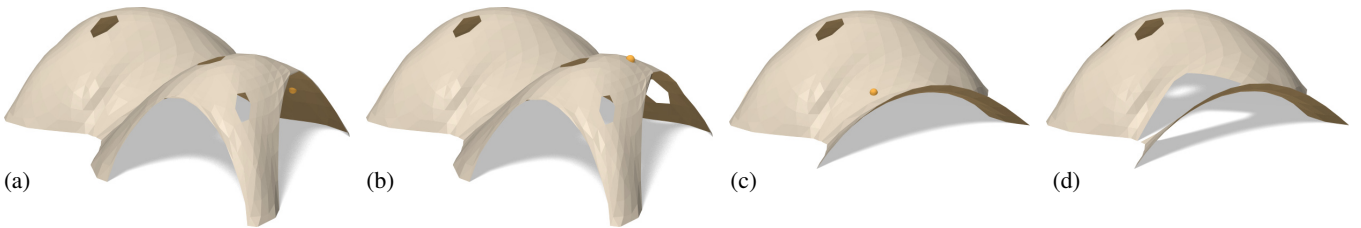


**Figure 13:** Destruction sequence. We simulate removing a part of masonry and the falling off of further pieces which are no longer supported after removal. This is done by deleting the 1-neighborhood of a vertex (shown in yellow) and solving for a new thrust network in compressive equilibrium close to the original reference surface. We delete those parts of the network which deviate too much and are no longer contained in the masonry hull, and iterate. (a) For this example, removing a certain small number single bricks does not affect stability. (b) Removal of material at a certain point will cause a greater part of the structure to collapse, as seen in (c). (d) shows the result after one more removal (all images show the respective thrust networks, not the reference surface).

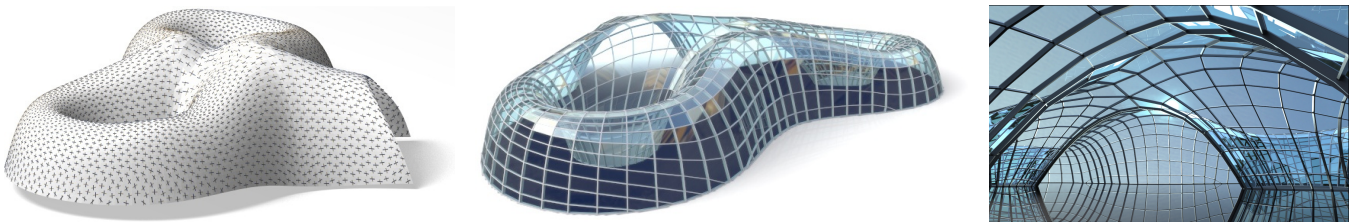


**Figure 14:** Planar quad remeshing of the surface of Figure 8. Left: Principal directions. Center: The result of optimization is a self-supporting PQ mesh, which guides a moment-free steel/glass construction. Right: Interior view.

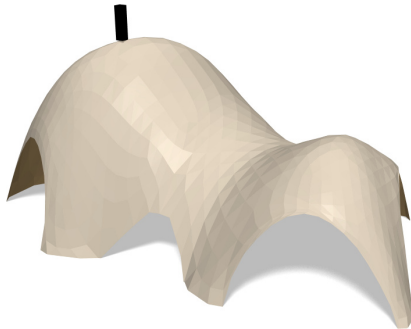


**Figure 15:** Testing stability. This self-supporting surface of length 24 m is imagined as masonry of thickness 0.1 m. It possesses a thrust network inside the masonry hull if – for the sake of example – a load of 900 kg (shown in black) is applied to a certain vertex. This means that the surface is still stable after that load is applied (N.B. This method of testing is rather conservative).

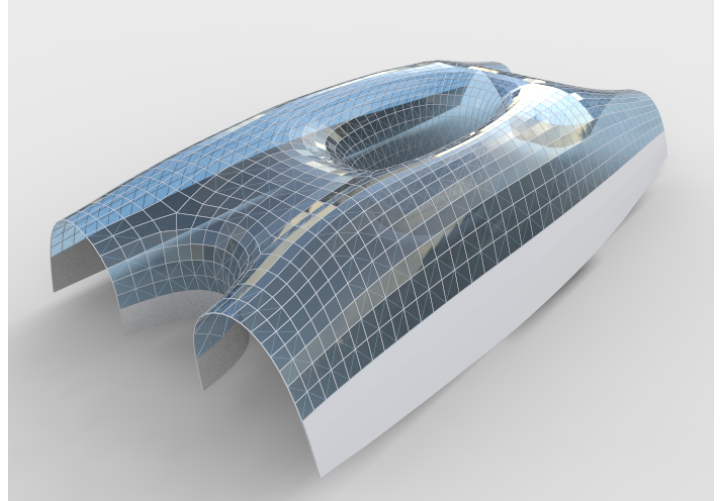


**Figure 16:** Glass as a structural element can support stresses up to, say, 30 MPa. We propose a steel/glass construction which utilizes the structural properties of glass by first solving for a self-supporting thrust network such that forces do not exceed the maximum values, and subsequent remeshing of this surface by a planar quad mesh (not necessarily self-supporting itself). Since this surface is very close to a self-supporting shape, joints will experience low bending and torsion moments.